Short-Term Functional Adaptation of Aquaporin-1 Surface Expression in the Proximal Tubule, a Component of Glomerulotubular Balance

Marcus Pohl,* Qixian Shan,† Thomas Petsch,* Beata Styp-Rekowska,‡ Patricia Matthey,§ Markus Bleich,† Sebastian Bachmann,* and Franziska Theilig*§

*Institute of Anatomy, Charité Universitätsmedizin, Berlin, Germany; †Institute of Physiology, Kiel University, Kiel, Germany; ‡Institute of Anatomy, University of Bern, Bern, Switzerland; and §Institute of Anatomy, Department of Medicine, University of Fribourg, Fribourg, Switzerland

ABSTRACT

Transepithelial water flow across the renal proximal tubule is mediated predominantly by aquaporin-1 (AQP1). Along this nephron segment, luminal delivery and transepithelial reabsorption are directly coupled, a phenomenon called glomerulotubular balance. We hypothesized that the surface expression of AQP1 is regulated by fluid shear stress, contributing to this effect. Consistent with this finding, we found that the abundance of AQP1 in brush border apical and basolateral membranes was augmented >2-fold by increasing luminal perfusion rates in isolated, microperfused proximal tubules for 15 minutes. Mouse kidneys with diminished endocytosis caused by a conditional deletion of megalin or the chloride channel ClC-5 had constitutively enhanced AQP1 abundance in the proximal tubule brush border membrane. In AQP1-transfected, cultured proximal tubule cells, fluid shear stress or the addition of cyclic nucleotides enhanced AQP1 surface expression and concomitantly diminished its ubiquitination. These effects were also associated with an elevated osmotic water permeability. In sum, we have shown that luminal surface expression of AQP1 in the proximal tubule brush border membrane is regulated in response to flow. Cellular trafficking, endocytosis, an intact endosomal compartment, and controlled protein stability are the likely prerequisites for AQP1 activation by enhanced tubular fluid shear stress, serving to maintain glomerulotubular balance.

Aquaporins are small integral membrane proteins that function as molecular water channels in plasma membranes.[1] Their permeability depends on the properties of the pore formed by the different channel isoforms and their abundance within the cell membrane. Aquaporin-1 (AQP1) is expressed in various cell types, including renal epithelial cells.[2,3] In the proximal nephron, fluid reabsorption is primarily driven by transcellular transport of solutes, basolateral cycling of Na^+, and secondary movement of water through transcellular and paracellular pathways.[4–6] High proximal tubular water permeability is, thus, tightly coupled to solute fluxes, which make up approximately 60% of the reabsorption along the nephron.[7] AQP1 is the major water channel of the proximal tubule. It is densely expressed in the brush border

membrane (BBM) and also lines the basolateral membrane.[8] Its exclusive role for transcellular osmotic water permeability has been shown in AQP1-deficient mice.[9–11] The high abundance of AQP1 in the BBM and especially, its insensitivity to vasopressin indicated a constitutive expression mode.[12] It has, however, been established that the proximal tubule

Correspondence: Prof. Franziska Theilig, Department of Medicine, University of Fribourg, Route Albert-Gockel 1, 1700 Fribourg, Switzerland. Email: franziska.theilig@unifr.ch

adapts rapidly to changes in electrolyte and fluid reabsorption to either prevent loss or retain sodium and water during variations of GFR. The direct positive effect of tubular flow rate on tubular reabsorption in the short term has been referred to as the glomerulotubular balance (GTB). On the basis of studies using micropuncture and microperfused proximal tubules, GTB has been defined as part of a feedback system that maintains a constant fractional reabsorption.[13–15] GTB is, in part, related to the major luminal sodium transporter of the proximal tubule, Na^+/H^+-exchanger-3 (NHE3). Tubular fluid shear stress (FSS), caused by increased flow, was shown to augment transport activity of NHE3 in the short term.[16,17] Less is known about the regulation of AQP1. Assuming that FSS regulates AQP1 trafficking in the short term in the context of GTB, we studied the distribution of the channel using isolated, microperfused proximal segments as well as opossum kidney cells (OKCs) stably transfected with AQP1. To gain mechanistic insight, the effects of cyclic nucleotides were studied in parallel to FSS. The ubiquitination of AQP1 was determined as a parameter for protein stability, and changes in transmembrane water permeability were established. The role of endocytosis in trafficking of AQP1 between BBM and apical cell pole was studied in mouse models with impaired endocytosis. Our observations suggest that, in the proximal tubule, AQP1 surface expression and stability rapidly adapt to changes in FSS as part of the functioning of the GTB.

RESULTS

Modulation of AQP1 Distribution by Flow Rate in Isolated–Perfused Proximal Tubule

To assess the effect of tubular flow on the abundance of AQP1 in the BBM and the underlying apical cell membrane, we performed immunocytochemistry in freshly prepared, isolated–perfused proximal tubular S2 segments. Flow was controlled by perfusion pressure and categorized by the inner diameter of the tubule; it was set at approximately 10 μm for low flow and 20 μm for high flow. These diameters correspond to flow rates of <5 and >25 nl/min.[17,18] Duration of the perfusion was 15 minutes throughout. Morphologic analysis revealed an intact structure of the tubules in both conditions (Figure 1, A and B). Ultrastructural evaluation of AQP1 immunogold signal showed significant increases under high-flow compared with low-flow rates (2.1-fold in the BBM, 3.4-fold in the subcellular compartment, and 2-fold in the basolateral cell membrane; $P<0.05$) (Figure 1, C–E). Control immunofluorescence staining displayed regular distribution of AQP1 in the BBM and the basolateral membrane after perfusion (low-flow condition) (Figure 1F).

Effect of Impaired Endocytosis on AQP1 Distribution in Mouse Proximal Tubule

Apical membrane distribution of AQP1 was studied in mice with impaired endocytosis caused by the conditional knockout of megalin (Lrp2^{fl/fl};apoE[Cre]). Owing to mosaic expression, these mice permit a cell-autonomous analysis of the defect with normal,

megalin-positive proximal tubule cells performing fluid-phase endocytosis located next to megalin-deficient cells incapable of endocytosis.[19] Triple-labeling immunohistochemistry showed complementary AQP1 staining patterns between horseradish peroxidase (HRP)/megalin-positive and HRP/megalin-deficient cells with a clear-cut, strong increase in signal intensity in the BBM of megalin-deficient cells (Figure 2A). Basolateral AQP1 distribution was not affected by HRP/megalin deficiency (Figure 2A). Ultrastructurally, AQP1 immunogold staining was found in the BBM and the subapical endomembrane compartment containing endosomal vesicles and dense apical tubules (also termed recycling endosomes)[19] as well as along the basolateral membrane of megalin-positive cells (Figures 1 and 2B). Compared with the latter, the megalin-deficient cells, identified by the absence of dense apical tubules, displayed a 107%±17% higher AQP1 signal in the BBM ($P<0.001$) along with reduced signal in the subapical compartment (−48%±7%; $P<0.001$) (Figure 2C). To confirm the immunohistochemical data, Western blots from cortical BBM preparations of LRP2^{fl/fl} and Lrp2^{fl/fl};apoE[Cre] mice were performed (Figure 2D). Megalin abundance in the BBM was decreased (−70%±17%; $P<0.005$), and AQP1 abundance, with signals of the two different bands pooled, was 92%±32% higher in Lrp2^{fl/fl};apoE[Cre] than control Lrp2^{fl/fl} mice ($P<0.005$).

To further validate the role of endocytosis in AQP1 distribution, mice with conditional knockout of ClC-5 (Clcn5[fl/y]; villin[Cre]), resulting in mosaic expression of the channel, were used. ClC-5–negative proximal tubule cells reveal intact endocytic machinery but decelerated endocytic uptake.[20] These cells showed reduced HRP uptake (Figure 2E). Here again, ClC-5–deficient cells showed higher AQP1 signal intensity in the BBM than ClC-5–positive cells, with basolateral signal remaining unaffected. Corresponding AQP1 immunogold signal was increased by 103%±45% in the BBM and decreased by 51%±22% in the subapical compartment of ClC-5–negative cells ($P<0.001$) (Figure 2, F and G). Western blots showed decreased ClC-5 signal (−60%±5%) and 93%±36% higher AQP1 signals in the BBM fractions of Clcn5[fl/y];villin[Cre] compared with control Clcn5[fl/y] mice ($P<0.01$) (Figure 2H). Full knockout mice (Clcn5[−/y]) showed complete loss of ClC-5 and 150%±50% higher AQP1 signals compared with wild-type mice (Clcn5[+/y]) ($P<0.001$). Generally, AQP1 mRNA levels were not different among the compared groups (Supplemental Table 1). Together, these results show that the amount of surface-expressed AQP1 in the proximal tubule depends on the integrity of endocytotic pathways determined by megalin and ClC-5.

Experimentally Induced Redistribution of AQP1 in Cultured Proximal Tubule Cells

OKCs were stably transfected with rat AQP1 cDNA (AQP1-OKC). The cells were polarized, and they displayed focal areas of apical microvilli and a central cilium (Figure 3, Supplemental Figure 1). They expressed immunoreactive AQP1 at several molecular mass levels, with a minor 28-kDa band and major 35- to 45-kDa bands likely representing differences in glycosylation. To study trafficking of AQP1 in these cells, orbital FSS
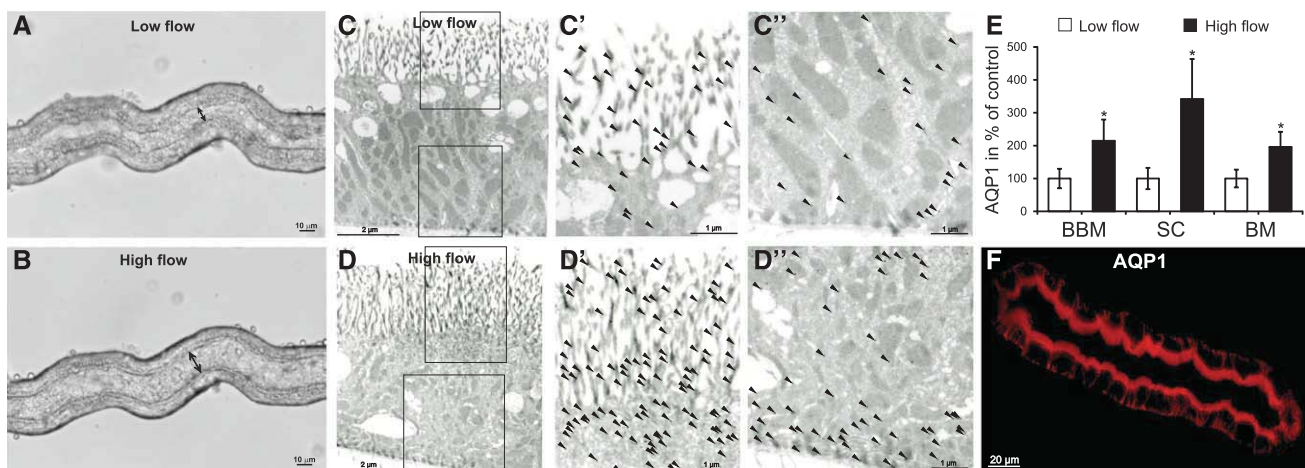
Figure 1. Effects of low and high luminal flow on AQP1 expression in isolated–perfused proximal tubules. (A and B) Freshly isolated tubules perfused at (A) low (<5 nl/min) or (B) high (>25 nl/min) perfusion rate for 15 minutes. Note the difference in tubule inner diameter (arrows). (C–E) Immunogold labeling of AQP1 and signal quantification in the BBM, subapical compartment (SC), and basolateral membrane (BM) of tubules after low- or high-flow perfusion. Insets are presented in greater detail in C′ and C″ for C or D′ and D″ for D. Gold particles are marked by arrowheads. Values are means±SDs; n=5–7 tubules for each condition. *P<0.01 by ANOVA. (F) Overview of AQP1 immunofluorescence staining in an isolated–perfused proximal tubule after low-flow perfusion, showing regular distribution of AQP1.

(induced by an orbital shaker adjusted to 1-Hz movements) condition was administered to the monolayers, and the established second messengers, guanosine 3′,5′-cyclic monophosphate (cGMP; 100 μmol 8-bromo-cGMP) and cAMP (100 μmol 8-bromo-cAMP), were added for 1 hour. Cell surface biotinylation, streptavidin-based immunoprecipitation, and Western blot analysis revealed significant increases in AQP1 signals in all three experimental settings compared with the control condition; there were no significant differences between the experimental values (Figure 3, A and C). The intracellular pool of AQP1 of the nonbiotinylated fractions remained unchanged under the above-mentioned conditions (Figure 3B). Confocal imaging was in good agreement with these data, showing increased AQP1 abundance in the apical microvilli on administration of FSS, cGMP, or cAMP (Figure 3D). Increased AQP1 abundance in the BBM, provoked by these stimuli, may, therefore, reflect redistribution and apical trafficking of AQP1 to the surface of AQP1-OKCs, although additional effects, potentially induced by altered protein turnover rate, have to be considered as well.

Experimentally Induced Changes in AQP1 Protein Turnover and Ubiquitination in Cultured Proximal Tubule Cells

To estimate changes in AQP1 protein turnover rate under experimental conditions, AQP1-OKCs were metabolically labeled using the [35S]methionine labeling technique followed by anti-AQP1 immunoprecipitation. After labeling (pulse), cells were then subjected to control or FSS conditions. Cells were lysed at a baseline time point (0) and after 1, 2, and 4 hours (time points of chase). Subsequently, protein was obtained by immunoprecipitation and separated by SDS-PAGE,

and the dried gels were examined by autoradiography (Figure 4A). Significant increases were recorded in the FSS group at 2 and 4 hours. The ubiquitination status of AQP1 was estimated in AQP1-OKCs, in which FSS (1 hour; <2 dynes/cm^2) was induced or cGMP or cAMP (8-bromo-cGMP and 8-bromo-cAMP, respectively; each 100 μmol for 1 hour) was added; samples were compared with untreated controls. Cells were then lysed, and AQP1 immunoprecipitates were obtained and probed for AQP1 and ubiquitin by Western blot (Figure 4, B and C). No AQP1 was detected after immunoprecipitation with rabbit IgG. AQP1 signals were increased throughout (Figure 4B). Immunoblotting for ubiquitin revealed discrete bands representing ubiquitinated AQP1. To estimate the quantities of ubiquitinated AQP1, signals were referred to total AQP1 abundances; values revealed massive decreases throughout the experimental conditions (Figure 4C). These results suggest that, in addition to AQP1 trafficking to the apical membrane, FSS, or second messengers, cGMP and cAMP may reduce AQP1 protein turnover and enhance AQP1 stability by reducing its ubiquitination.

Experimentally Induced Changes in Water Permeability of Cultured Proximal Tubule Cells

To estimate osmotic water permeability in AQP1-OKC in relation to the amount of surface-expressed AQP1, we applied the calcein fluorescence quenching method. Here, the magnitude of change in cellular calcein fluorescence correlates with the relative change in cell volume in response to reduced solution osmolality.[21] A significant increase in the magnitude of change in calcein fluorescence, revealed by determining the reciprocal exponential time constant ($1/\tau$), was found in AQP1-OKC in which FSS (1 hour; <2 dynes/cm^2) was
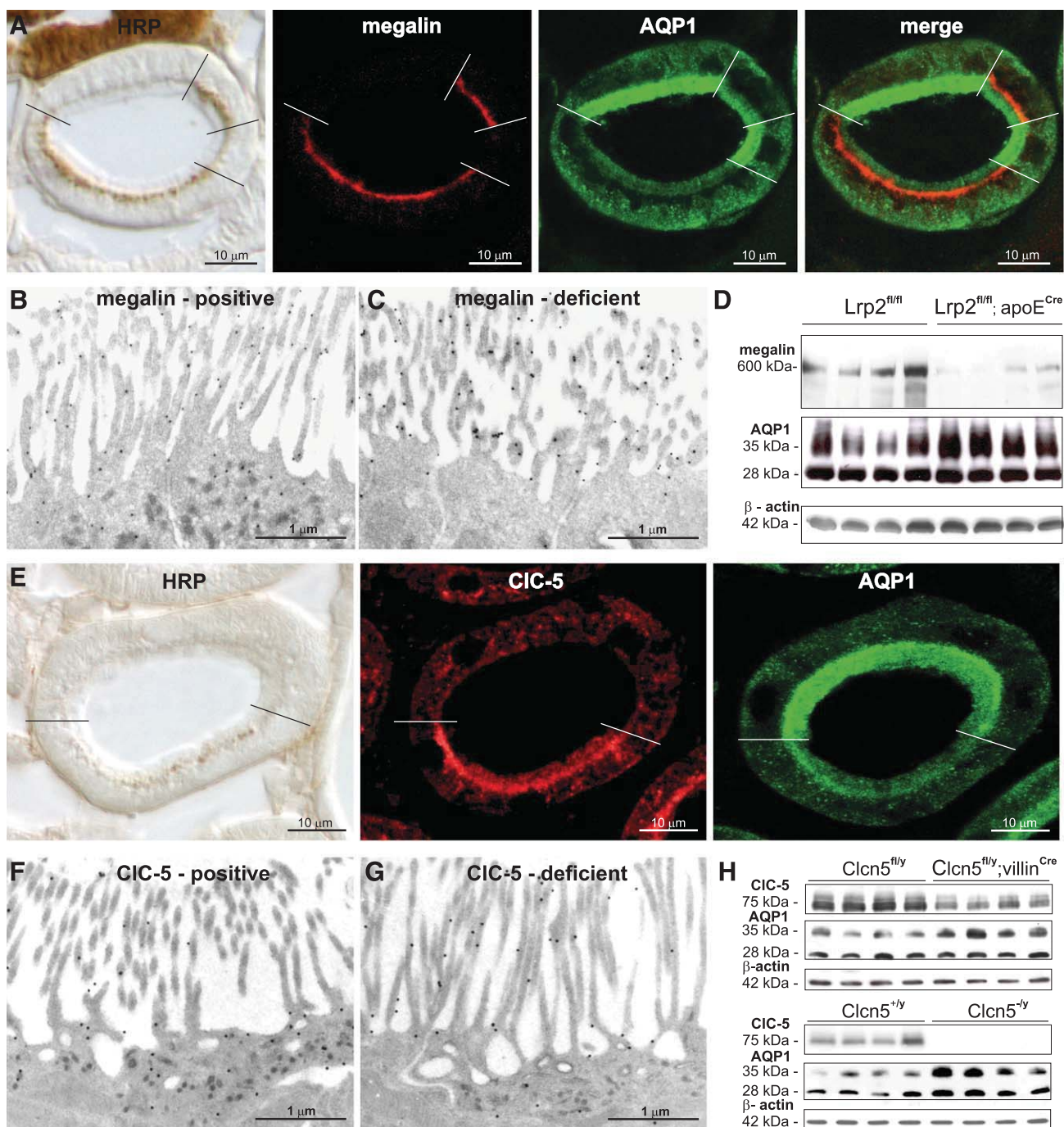
Figure 2. Renal AQP1 distribution in mice with partial deficiency of megalin or Clcn5. (A) Triple-labeling immunohistochemistry showing complementary patterns of AQP1 BBM signal and endocytosis in the S2 proximal tubule with mosaic deficiency of megalin (Lrp2^{fl/fl}; apoE[Cre] conditional megalin knockout), with HRP marking intact endocytosis (dark brown signal; 5 minutes after injection), megalin (red immunofluorescence), AQP1 (green immunofluorescence), and the respective merge image. Boundaries between megalin-positive and megalin-deficient cells are indicated by black and white bars. (B) AQP1 immunogold staining shows balanced expression in the BBM and subapical compartment of megalin-expressing cells identified by an intact endosomal apparatus. (C) AQP1 signal is absent from the subapical compartment but enhanced in the BBM of megalin-deficient cells, displaying a reduced endosomal apparatus. (D) Representative Western blots of megalin, AQP1, and β-actin as loading controls in BBM preparations from control versus conditional megalin knockout mouse kidneys. (E) Complementary signals for AQP1 in the BBM and endocytosis in the S2 proximal tubule with mosaic deficiency of ClC-5 (Clcn5[fl/y];villin[Cre] conditional knockout), with HRP marking intact endocytosis (dark brown signal; 5 minutes after injection), ClC-5 (red), and AQP1 (green). Boundaries between ClC-5–positive and ClC-5–deficient cells are indicated by black and white bars. (F) Compared with ClC-5–positive cells, (G) immunogold labeling of AQP1 shows increased expression in the BBM
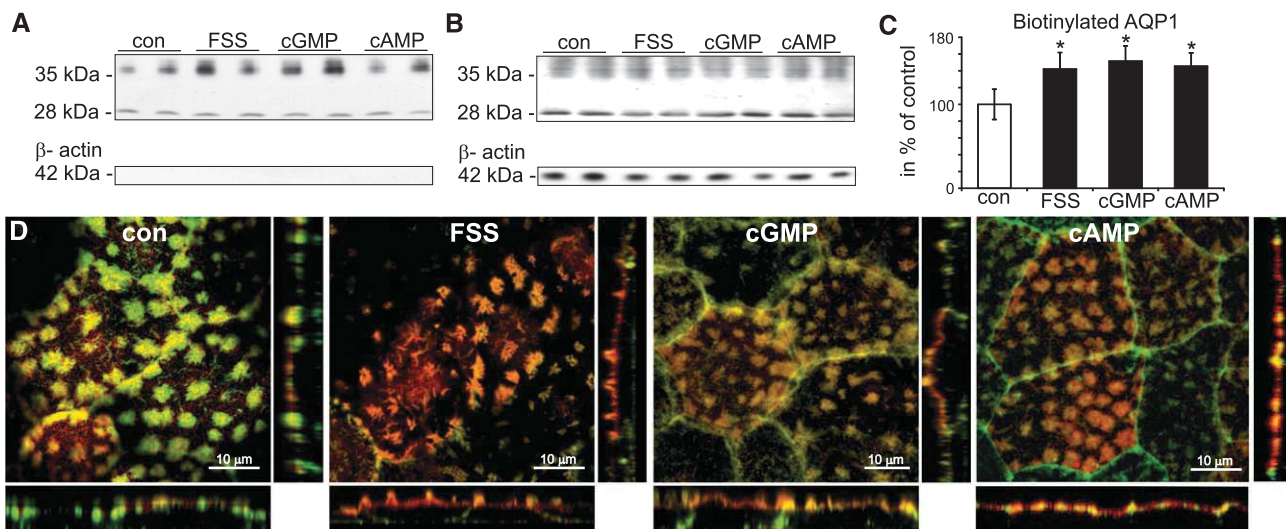
Figure 3. Experimentally induced redistribution of AQP1 in cultured proximal tubule cells. OKC cells stably transfected with rat AQP1 cDNA (AQP1-OKC) were evaluated. (A–C) To show cell luminal expression of AQP1 by surface biotinylation and streptavidin-based immunoprecipitation techniques, immunoblotting of (A) biotinylated and (B) nonbiotinylated fractions is shown in controls (con), on induction of FSS (1 hour; <2 dynes/cm^2), and after addition of cGMP or cAMP (8-bromo-cGMP and 8-bromo-cAMP, respectively; each 100 μmol for 1 hour); β-actin bands serve as loading controls. Representative duplicates are shown. (C) Densitometric evaluation of the biotinylated fractions shows increases of cell surface-expressed AQP1 in the experimental conditions; the nonbiotinylated intracellular fractions reveal no changes. (D) Immunohistochemical analysis of AQP1-OKC showing AQP1 (red signal) and actin (green signal) immunofluorescence; apical microvilli, typically occurring as clusters, display merged signals with a red shift in the experimental conditions. Values are means±SDs from *n*=12 independent experiments. *P<0.001.

induced or cGMP or cAMP (8-bromo-cGMP and 8-bromo-cAMP, respectively; each 100 μmol for 1 hour) was added (Figure 5A). There were significant increases in all three conditions compared with the control level; differences between the distinct stimuli were not statistically significant. We further assessed how various intensities of laminar FSS may alter osmotic water permeability; $1/\tau$, reflecting osmotic water permeability, reached its maximum at 1 dyne/cm^2 and decreased to near control levels at 4 dynes/cm^2, revealing a biphasic course (Figure 5B). Original data are depicted in Supplemental Figure 2. Our findings suggest an increase in proximal tubule water permeability after dynamic redistribution of functional AQP1 toward the BBM. The application of laminar FSS may have the same effect.

DISCUSSION

The proximal tubule reabsorbs the bulk of filtered water and solutes, playing a key role in body fluid and BP homeostasis. It also adapts to changing glomerular flow rates by increasing or decreasing its salt and water reabsorption through the GTB, and a near-linear relationship between the filtered volume and tubular reabsorption has been established.[22] Absence of the main

proximal tubular sodium transporter, NHE3, or the principal water channel, AQP1, did not entirely abolish GTB but significantly reduced the slope of flow-dependent volume absorption.[16,18,23,24] We aimed to resolve whether the surface expression of AQP1 may be altered in the short term by inducing changes in luminal flow rate and FSS. The selected flow rates for the isolated, microperfused tubules reflected the end proximal physiologic range of 5–30 nl/min.[25] Our data support the concept that the cell may adjust AQP1 membrane density within the short term to augment its transepithelial water movement, because at high-flow rate, AQP1 surface expression, as established by immunogold labeling, was increased apically at the BBM as well as basolaterally after 15 minutes. This concept was indirectly supported by models in which a downregulated AQP1 surface expression coincided with reduced GFR.[26,27] It is not clear at all how the apical side of the cell as the likely site of perception of altered flow conditions transmits its signal to the basolateral side to increase the membrane density of AQP1. Therefore, our study was focused primarily on the BBM and subapical compartment of the proximal tubule. The rapid flow-induced increase in apical AQP1 BBM expression implies that trafficking mechanisms or changes in protein stability have to be considered. Trafficking of AQP1 from an intracellular compartment to the apical plasma

and a reduced number of gold granules in the subapical compartment of ClC-5–deficient cells. (H) Representative Western blots of ClC-5, AQP1, and β-actin of the BBM preparations from kidney extracts of (upper panel) control versus conditional ClC-5 knockout as well as (lower panel) control and ClC-5 full knockout mouse kidneys.
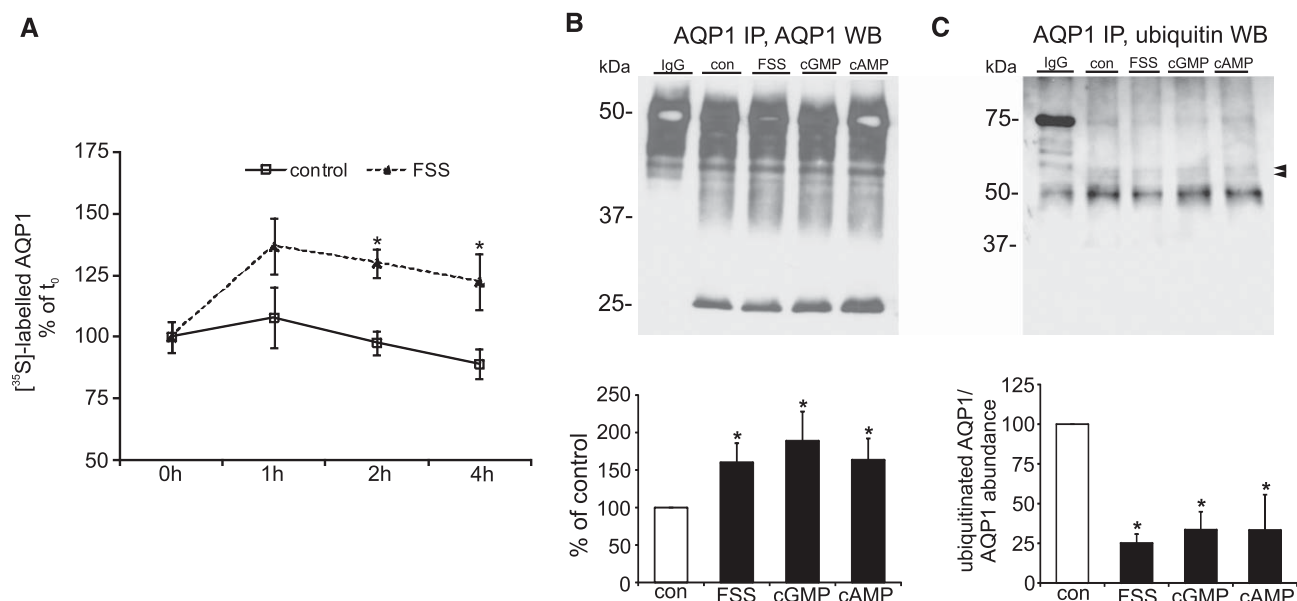
Figure 4. AQP1 protein turnover and ubiquitination in cultured proximal tubule cells. (A) Estimation of AQP1 protein turnover rate. AQP1-OKCs were FCS and methionine depleted overnight and then incubated with [^{35}S]methionine for 2 hours. Chase was performed at baseline and after 1, 2, and 4 hours under control and FSS conditions. The SDS-PAGE gel shows the immunoprecipitated AQP1 bands differing in glycosylation and an IgG control band. The densitometric values, as determined by autoradiography using a phosphoimager, are plotted along the time axis. Values are expressed as the percentage of the baseline time point (0 hours) and are means±SDs with $n=4$ independent experiments. *$P<0.005$. (B) Abundance and (C) ubiquitination of AQP1 obtained by immuno-precipitation from AQP1-OKCs after control (con), FSS (1 hour; <2 dynes/cm^2) conditions, or addition of cGMP or cAMP (8-bromo-cGMP and 8-bromo-cAMP, respectively; each 100 μmol for 1 hour). No AQP1 was obtained after immunoprecipitation with IgG. Densitometric analysis confirms increases of signals in the AQP1 blots, including distinct glycosylation patterns in all of the experimental conditions; bands were pooled to evaluate. To estimate ubiquitination, the same immunoprecipitates used in B were probed in C. Arrowheads mark the positions of discrete bands approximately ranging between 50 and 60 kD; they are consistent with the addition of two ubiquitin moieties. Densitometric evaluation of the blots shows reduced ubiquitination of AQP1. Values for ubiquitinylated AQP1 are referred to the respective levels of immunoprecipitated AQP1, and they are means±SDs from $n=4–5$ independent experiments in each condition. IP, immunoprecipitation; WB, Western blot. *$P<0.01$.

membrane has earlier been shown using heterologous green fluorescent protein-tagged AQP1 in HEK293 cells as well as murine cholangiocytes on hormonal stimuli.[28] Mosaic cellular deletion in the conditional mouse models for megalin and ClC-5 deficiency permitted us to analyze AQP1 trafficking pathways in more detail, showing intact cells located side by side with cells with impaired endocytic function in the proximal tubule. Megalin-deficient cells lack much of the apical endosomal apparatus, whereas ClC-5–deficient cells have decelerated endocytosis caused by reduced acidification of endosomes.[19,29,30] Both defects clearly showed that AQP1 was accumulated in the BBM when endocytosis was impaired. This result was probably on the basis of the defect of retrieval functions, which was shown earlier for the phosphate transporter NaPi-IIa.[19] However, AQP1 immunogold signal was not only found in absorptive but also, recycling endosomes. Altered retrieval may, therefore, be directly affected by malfunction of the absorptive apparatus, but indirectly, it may also depend on protein recycling vesicles. They determine the BBM presence of megalin, and in case of a functionally relevant interaction of megalin and AQP1, the scavenger receptor itself may as well determine AQP1 surface expression.[19,20] The presence of AQP1 in

recycling endosomes of intact cells further suggests that a pool of inactive AQP1 may be ready for apical shuttling after stimulus, which was shown before for NHE3, with the likely involvement of the cytoskeletal proteins actin and tubulin and the motor proteins kinesin and dynein.[31] This scenario may well apply for our observations.

In the kidney, many physiologic processes are mediated by cellular signal cascades involving cyclic nucleotides and specific protein kinases to provide or control the phosphorylation of membrane proteins. This finding has been well established for the regulation and function of AQP2 in the collecting duct.[32] Phosphorylation of AQP1 was shown in the context of its trafficking and insertion into the membrane,[33] and potential phosphorylation sites for protein kinase A , protein kinase C, and casein kinase II have been identified for AQP1.[33] Recent data have shown that a hypotonicity-induced translocation of AQP1 occurs within 30 seconds using an isolated cell system; mutation of known protein kinase C phosphorylation sites completely abolished this shift.[34] In this setting, transient receptor potential channels, Ca^{++}, and calmodulin were shown to be crucially involved.[34] In line with this context, the use of established pharmacologic stimuli and
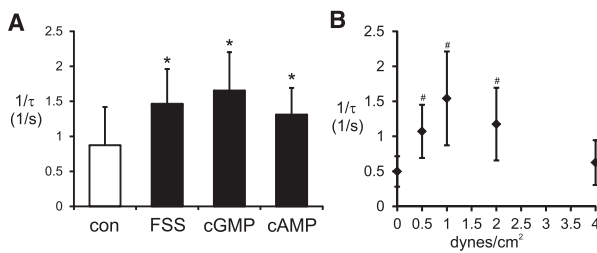
Figure 5. Osmotic water permeability in cultured proximal tubule cells. Osmotic cell swelling rates of AQP1-OKCs are shown in response to orbital FSS (1 hour; <2 dynes/cm²) or addition of cGMP or cAMP (8-bromo-cGMP and 8-bromo-cAMP, respectively; each 100 μmol for 1 hour) to show changes in osmotic water permeability. The calcein fluorescence quenching method was applied; the magnitude of change in calcein fluorescence is presented as reciprocal exponential time constants (1/τ) and corresponds to cell expansion in response to reduced solution osmolality. (A) Calcein-loaded cells show changes in calcein fluorescence on all three experimental conditions. (B) Cells grown in flow chambers were calcein loaded, and increasing intensities of laminar FSS were applied for 1 hour. Controls: no treatment (con) or 0 dyne/cm²; values are means±SDs from n=6 and n=5 independent experiments in each condition, respectively. *$P<0.05$ versus #$P<0.005$.

experimental models, including a *Xenopus laevis* oocyte expression system, has provided some evidence that both cyclic nucleotides, cAMP and cGMP, activate AQP1.[35,36] Other data have indicated a stimulatory role of cGMP on AQP1-dependent water transport in the eye.[37]

Our findings suggest that the signaling molecules cAMP and cGMP promote trafficking of AQP1 into the BBM of proximal tubular cells, and among the stimulated groups, no significant differences between the effects of the two nucleotides were evident. Because highly divergent findings of cAMP- and cGMP-triggered pathways have been reported with respect to other proximal tubular membrane proteins, such as NHE3, which among other characteristics, revealed a dose-dependent biphasic (*i.e.*, partly inhibited and partly stimulated) response on protein kinase A activation,[38] it is currently impossible to adequately assign our data to the detail of defined signaling cascades stimulating AQP1, and more work needs to be done in this respect. Orbital FSS produced similar changes as the cyclic nucleotides, and along same line, it may only be speculated whether a luminal stimulus may trigger one or both of the cyclic nucleotide pathways to promote AQP1 trafficking. Whether the primary stimulus is microvillous torque, which was discussed in the context of an NHE3 knockout mouse,[18] or whether bending of the primary cilium is the cause cannot be concluded from our data. In this context, the actin cytoskeleton has been identified as the transmitter for hydrodynamic torque mediating GTB[39]; one may speculate that the biphasic course of the response to laminar FSS shown in Figure 5B may indicate inadequate stress on the cytoskeleton and consequently, reduction of transmembrane water movement.

Finally, FSS, cAMP, and cGMP have all reduced the ubiquitination of AQP1 in our setting, suggesting that this effect increased

AQP1 protein stability, because regulated proteolysis is commonly achieved through the ubiquitin–proteasome pathway; in this respect, two potential ubiquitination sites (Lys-243 and Lys-267) were indicated in the AQP1 amino acid sequence using computational prediction of protein ubiquitination.[40] AQP1 availability also has elsewhere been shown to increase on the inhibition of its proteasomal degradation.[41] However, in the same context, hypertonic stress was shown to reduce ubiquitination of AQP1, leading to increased half-life of AQP1; like in our results, ubiquitin bands ranged between 50 and 60 kDa.[41] The regulatory role of varying protein stability has also been shown for AQP2.[42] Altered ubiquitination, as observed in our setting of stimulated AQP1-OKCs, could have contributed as well to part of the changes seen in the microperfused tubules.

In sum, we have shown that kidney proximal tubule cells have the capacity to adapt AQP1 membrane density to changes in luminal flow in the short term, which suggests that AQP1 is tightly regulated to achieve GTB in this segment. Endocytosis is an effective determinant in the control of apical AQP1 expression. Our study provides additional mechanistic information on FSS increasing AQP1 surface expression, potentially involved cyclic nucleotides and protein ubiquitination, and alterations in transmembrane fluid movement.

CONCISE METHODS

In Vitro Microperfusion of Proximal Tubule

Proximal tubules (S2 segments) were freshly isolated from C57/Bl6 mice (either sex, 6–8 weeks old) and perfused *in vitro* by a pressure-controlled, single-barreled concentric glass pipette perfusion system.[43] Dissected tubules were transferred onto the heated stage of an inverted microscope (Axiovert 10; Carl Zeiss), monitored, and measured by video imaging (Visitron Systems). Only tubules with an open solution outflow were accepted for the study. The luminal perfusion rates were adjusted by an automatic perfusion pressure control system (Department of Physiology, Kiel University) connected to the perfusion pipette. The low-flow condition was defined as the perfusion rate that constantly opened the tubule lumen to a diameter of approximately 10 μm. The perfusion rate that doubled the inner diameter was referred to as high flow. After continuous perfusion for 15 minutes, the tubules were fixed immediately within the perfusion system using 3% paraformaldehyde/0.05% glutardialdehyde in PBS for 5 minutes. After washing, tubules were embedded in 1% agar and then L.R. White hydrophilic resin (Polysciences). The use of mice was approved by Kiel University.

Animals and Treatments

Experiments were performed on male conditional megalin (Lrp2^{fl/fl}; apoE[Cre]) and conditional ClC-5 (Clcn5[fl/y];villin[Cre]) knockout mice.[29,44] The respective control littermates were Lrp2^{fl/fl} and Clcn5[fl/y], respectively. Additionally, ClC-5 knockout (Clcn5[−/y])[20] and wild-type (Clcn5[+/y]) mice were used. The respective mice were divided into two groups (n=12 each): one group for morphologic evaluation and one group for biochemical evaluation. Mice were allowed free access to standard chow and tap water. Mice were anesthetized by an intraperitoneal injection of

sodium pentobarbital (0.06 mg/g body wt) or 2.5% isoflurane inhalation. To visualize fluid-phase endocytosis, mice received 2.5 mg HRP (Sigma-Aldrich) 5 minutes before perfusion fixation (n=4 each). All experiments were conducted in accordance with the German Law for the Protection of Animals and approved by the Berlin Senate.

RNA Analyses by Real-Time PCR
Total RNA was isolated and reverse transcribed, and quantitative PCR using Taqman assay Mm00431834_m1 was performed as described.[45] Differences between values obtained for AQP1 and the housekeeping gene glyceraldehyde-3-phosphate dehydrogenase (ΔCt) were calculated and compared between groups.

Cell Culture, Constructs, Stable Transfection, and Treatments
OK cells were provided by Heini Murer. Cells were cultured at 37°C in 95% air/5% CO_2 in high-glucose (450 mg/dl) DMEM supplemented with 10% FBS, penicillin (100 units/ml), and streptomycin (100 μg/ml). OK cells were seeded on PET filters (0.4-μm pore size; Falcon) pretreated with Matrigel (BD Biosciences). Confluence was assessed by transepithelial resistance measurements and considered optimal for transport polarity studies when the resistance exceeded 160 Ohm·cm². For stable transfection and expression of AQP1, full-length rat AQP1 cDNA (RZPD) was subcloned into the mammalian expression plasmid by directional cloning of full-length rat AQP1 cDNA into the *Bam*HI and *Hin*dIII restriction sites of the eukaryotic vector pCDNA 3.1 (Invitrogen). OK cells were stably transfected with rat AQP1 pcDNA3.1 and selected by incubation with 0.4–2 mg/ml geneticin (G418; Sigma-Aldrich). After selection, AQP1-OKCs were cultured with standard medium supplemented with 0.4 mg/ml geneticin. AQP1-OKCs were stimulated with orbital FSS (1 hour), 100 μmol 8-bromo-cAMP and 500 μM 3-isobutyl-1-methylxanthine (IBMX), or 100 μmol 8-bromo-cGMP and IBMX (1 hour). FSS was applied to confluent cultures with the use of an orbital shaker in the incubator, which produces a nonuniform laminar shear, with the majority of cells being exposed to near-maximal (peak) shear stress (τ max). Orbital FSS can be calculated as shown in ref. 46, where a is the radius of orbital rotation (1.5 cm), Rho is the density of the culture medium (1.0 g/cm³), η is the viscosity of the medium (0.0075 dyne/s per centimeter²), and f is the frequency of rotation (1 Hz). In our experimental setting, we calculated τmax=2.0 dynes/cm². However, measurements of shear stress in the center and periphery revealed lower values than calculated.[46] Therefore, we can assume that the orbital FSS applied in our experimental setting was lower than 2 dynes/cm².

Fixation and Tissue Processing for Immunohistochemistry and Immunoblotting
Kidneys were shock-frozen for biochemical evaluation or perfused retrogradely using 3% paraformaldehyde for morphology or immunohistochemistry as described.[47] For electron microscopy, tissues were embedded in L. R. White resin. For isolation of cortical BBMs, kidney cortex was homogenized in isolation buffer and processed as described.[19] Total protein concentration was measured using the Pierce BCA Protein Assay Reagent Kit (Pierce) and controlled by Coomassie staining.

SDS-PAGE and Immunoblotting
Proteins were solubilized, and SDS-PAGE was performed on 8%–10% polyacrylamide gels. After electrophoretic transfer of the proteins to nitrocellulose membranes, equity in protein loading and blotting was verified by membrane staining using 0.1% Ponceau red. Membranes were probed with primary antibodies and then exposed to HRP-conjugated secondary antibodies (DAKO). Immunoreactive bands were detected by chemiluminescence (Amersham Pharmacia). Densitometric evaluation was performed by BIO-PROFIL Bio-1D image software (Vilber Lourmat). All parameters were normalized to β-actin abundance.

Antibodies
We used previously well characterized antibodies: rabbit anti-AQP1 (Alpha Diagnostics), mouse monoclonal anti–β-actin (Sigma-Aldrich), guinea pig anti-megalin,[48] and rabbit anti–ClC-5.[44]

Immunoprecipitation
AQP1-OKCs were resuspended in coimmunoprecipitation buffer (25 mM Tris-HCl, pH 7.6, 150 mM NaCl, 1% NP-40) supplemented with protease inhibitor cocktail (Roche Diagnostics), 1 μg/ml ubiquitin aldehyde, and 5 mM N-ethylmaleimide to limit protein degradation and deubiquitination as well as phosphatase inhibitors (100 mM NaF, 10 mM di-Na-pyrophosphate, and 1 mM Na-orthovanadate). Insoluble material was removed, and 500 μg protein per sample was incubated with 4 μg rabbit IgG (The Jackson Laboratory) or polyclonal AQP1 at 4°C added with protein G Dynabeads (Invitrogen) for 4 hours. The immunoprecipitated samples were washed two times with coimmunoprecipitation buffer and one time with RIPA buffer of 25 mM Tris-HCl, pH 7.6, 150 mM NaCl, 1% NP-40, 1% sodium deoxycholate, and 0.1% SDS supplemented with protease inhibitor cocktail, 5 mM N-ethylmaleimide, 100 mM NaF, 10 mM di-Na-pyrophosphate, and 1 mM Na-orthovanadate. Elution of proteins was carried out for 30 minutes at 37°C, and 1/10th of the eluate was subjected to SDS-PAGE and Western blot analysis for AQP1; the rest were subjected to SDS-PAGE and Western blot using mouse monoclonal anti-ubiquitin (FK2; EMD Millipore) to determine ubiquitinylation of AQP1.

Immunohistochemistry
Cryosections were blocked with 5% skim milk/PBS and incubated with the respective primary antibody followed by the suitable cy-2– or cy-3–coupled secondary antibody (Dianova). Double-antibody staining procedure was controlled by parallel incubation of consecutive sections, each probed only with one single antibody. Sections were analyzed using a multilayer confocal scanning microscope (LSM5 Exciter; Carl Zeiss). For immune electron microscopy, ultrathin sections of L.R. White-embedded tissue were blocked with 5% skim milk/PBS and incubated with anti-AQP1 followed by incubation with 10 nm gold particle-coupled anti-rabbit antibody. Sections were visualized using a Carl Zeiss EM 906 and morphometrically analyzed using the MetaVue (Molecular Devices) software. Gold particles were counted (*1*) per area of BBM, (*2*) in the subapical membrane region ranging between the base of the microvilli and the basal onset of the endosomal compartment, and (*3*) in the basolateral membrane region ranging from its apical end to the basement membrane.

Cell Surface Biotinylation
Surface biotinylation was carried out to obtain luminally expressed protein in confluent AQP1-OKCs; 24 hours before experimental

stimulation, cells were FCS depleted and stimulated for 1 hour with orbital FSS, 8-bromo-cAMP and IBMX, or 8-bromo-cGMP and IBMX (see above for details). Cells were subsequently washed with ice-cold PBS and surface biotinylated (Cell Surface Protein Isolation Kit; Pierce). The isolation and separation of cell surface and intracellular proteins were carried out according to the manufacturer's instruction. Eluted proteins were analyzed by immunoblotting using anti-AQP1 and anti–β-actin antibodies.

Metabolic Labeling

AQP1 protein turnover rate was estimated in confluent AQP1-OKCs. Cells were serum, methionine, and cysteine starved overnight and then incubated with 10 μCi/ml [^{35}S]methionine (Hartmann Analytics) for 2 hours (pulse). Cells were thoroughly washed and analyzed at baseline and on orbital FSS or control conditions for 1, 2, and 4 hours (Chase). After harvesting the cells for immunoprecipitation, cells were lysed using coimmunoprecipitation buffer, and 200 μg protein was incubated with 2 μg rabbit IgG (The Jackson Laboratory) or polyclonal anti-AQP1 at 4°C added with protein G Dynabeads overnight. Precipitates were washed one time with coimmunoprecipitation buffer and two times with RIPA buffer followed by elution for 30 minutes at 37°C and separation by SDS-PAGE. Gels were dried, and radioactivity was determined by using a phosphoimager (Amersham Pharmacia).

Water Permeability Measurements

Water permeability assays were performed as described previously with some modifications.[21] Confluent AQP1-OKCs grown on glass Petri dishes or for flow chamber experiments, μ-Slide I 0.8 Luer (IBIDI) were FCS depleted overnight and loaded with calcein by incubating cells for 30 minutes with 2 μM calcein-acetoxymethylester (Invitrogen). After washing, cells were stimulated for 1 hour with orbital FSS, 8-bromo-cAMP and IBMX, 8-bromo-cGMP and IBMX, or various rates of laminar FSS profile applied by moving a cell medium with defined viscosity through a pressure-driven flow chamber (IBIDI). Laminar FSS profiles applied were control at 0 dyne/cm^2 and FSS of 0.5, 1, 2, and 4 dynes/cm^2. FSS of 0.2 dynes/cm^2 corresponded to the reference state of 5 nl/min in mouse proximal tubule *in vivo*.[23] The rate of change of calcein fluorescence intensity inside the cells was monitored using confocal microscopy (SP5; LEICA or Live510Duo; Carl Zeiss) after exposing cells to hypertonic PBS (500 mosM, solution supplemented with sucrose) followed by switching to hypotonic PBS (150 mosM). Osmolality was controlled by a freezing-point depression osmometer (FISKE). The rate of change of cell volume is presented as the reciprocal exponential time constant ($1/\tau$), which is proportional to osmotic water permeability, where τ is the time needed from the beginning of osmotic water switch to the point when the cytoplasmic calcein fluorescence reached its maximum.

Presentation of Data and Statistical Analyses

Quantitative data are presented as means±SDs. For statistical comparison, the Mann–Whitney U test, t test, and where appropriate, ANOVA were used. When ANOVA was significant, a Tukey test for multiple comparisons was applied. P values<0.05 were considered statistically significant.

DISCLOSURES

None.

REFERENCES

1. Agre P: The aquaporin water channels. *Proc Am Thorac Soc* 3: 5–13, 2006
2. Verkman AS: Aquaporins at a glance. *J Cell Sci* 124: 2107–2112, 2011
3. Kortenoeven ML, Fenton RA: Renal aquaporins and water balance disorders. *Biochim Biophys Acta* 1840: 1533–1549, 2014
4. Larsen EH, Møbjerg N: Na+ recirculation and isosmotic transport. *J Membr Biol* 212: 1–15, 2006
5. Rosenthal R, Milatz S, Krug SM, Oelrich B, Schulzke JD, Amasheh S, Günzel D, Fromm M: Claudin-2, a component of the tight junction, forms a paracellular water channel. *J Cell Sci* 123: 1913–1921, 2010
6. Muto S, Hata M, Taniguchi J, Tsuruoka S, Moriwaki K, Saitou M, Furuse K, Sasaki H, Fujimura A, Imai M, Kusano E, Tsukita S, Furuse M: Claudin-2-deficient mice are defective in the leaky and cation-selective paracellular permeability properties of renal proximal tubules. *Proc Natl Acad Sci U S A* 107: 8011–8016, 2010
7. Nielsen S, Smith BL, Christensen EI, Knepper MA, Agre P: CHIP28 water channels are localized in constitutively water-permeable segments of the nephron. *J Cell Biol* 120: 371–383, 1993
8. Nielsen S, Frøkiaer J, Marples D, Kwon TH, Agre P, Knepper MA: Aquaporins in the kidney: From molecules to medicine. *Physiol Rev* 82: 205–244, 2002
9. Vallon V, Verkman AS, Schnermann J: Luminal hypotonicity in proximal tubules of aquaporin-1-knockout mice. *Am J Physiol Renal Physiol* 278: F1030–F1033, 2000
10. Ma T, Yang B, Gillespie A, Carlson EJ, Epstein CJ, Verkman AS: Severely impaired urinary concentrating ability in transgenic mice lacking aquaporin-1 water channels. *J Biol Chem* 273: 4296–4299, 1998
11. Schnermann J, Chou CL, Ma T, Traynor T, Knepper MA, Verkman AS: Defective proximal tubular fluid reabsorption in transgenic aquaporin-1 null mice. *Proc Natl Acad Sci U S A* 95: 9660–9664, 1998
12. Knepper MA, Wade JB, Terris J, Ecelbarger CA, Marples D, Mandon B, Chou CL, Kishore BK, Nielsen S: Renal aquaporins. *Kidney Int* 49: 1712–1717, 1996
13. Bartoli E, Conger JD, Earley LE: Effect of intraluminal flow on proximal tubular reabsorption. *J Clin Invest* 52: 843–849, 1973
14. Häberle DA, Shiigai TT, Maier G, Schiffl H, Davis JM: Dependency of proximal tubular fluid transport on the load of glomerular filtrate. *Kidney Int* 20: 18–28, 1981
15. Peterson OW, Gushwa LC, Blantz RC: An analysis of glomerular-tubular balance in the rat proximal tubule. *Pflugers Arch* 407: 221–227, 1986
16. Wang T: Flow-activated transport events along the nephron. *Curr Opin Nephrol Hypertens* 15: 530–536, 2006
17. Du Z, Yan Q, Duan Y, Weinbaum S, Weinstein AM, Wang T: Axial flow modulates proximal tubule NHE3 and H-ATPase activities by changing microvillus bending moments. *Am J Physiol Renal Physiol* 290: F289–F296, 2006

18. Du Z, Duan Y, Yan Q, Weinstein AM, Weinbaum S, Wang T: Mechanosensory function of microvilli of the kidney proximal tubule. *Proc Natl Acad Sci U S A* 101: 13068–13073, 2004

19. Bachmann S, Schlichting U, Geist B, Mutig K, Petsch T, Bacic D, Wagner CA, Kaissling B, Biber J, Murer H, Willnow TE: Kidney-specific inactivation of the megalin gene impairs trafficking of renal inorganic sodium phosphate cotransporter (NaPi-IIa). *J Am Soc Nephrol* 15: 892–900, 2004

20. Piwon N, Günther W, Schwake M, Bösl MR, Jentsch TJ: ClC-5 Cl- -channel disruption impairs endocytosis in a mouse model for Dent's disease. *Nature* 408: 369–373, 2000

21. Solenov E, Watanabe H, Manley GT, Verkman AS: Sevenfold-reduced osmotic water permeability in primary astrocyte cultures from AQP-4-deficient mice, measured by a fluorescence quenching method. *Am J Physiol Cell Physiol* 286: C426–C432, 2004

22. Schnermann J, Wahl M, Liebau G, Fischbach H: Balance between tubular flow rate and net fluid reabsorption in the proximal convolution of the rat kidney. I. Dependency of reabsorptive net fluid flux upon proximal tubular surface area at spontaneous variations of filtration rate. *Pflugers Arch* 304: 90–103, 1968

23. Duan Y, Weinstein AM, Weinbaum S, Wang T: Shear stress-induced changes of membrane transporter localization and expression in mouse proximal tubule cells. *Proc Natl Acad Sci U S A* 107: 21860–21865, 2010

24. Schnermann J, Huang Y, Mizel D: Fluid reabsorption in proximal convoluted tubules of mice with gene deletions of claudin-2 and/or aquaporin1. *Am J Physiol Renal Physiol* 305: F1352–F1364, 2013

25. Schnermann J, Briggs JP: The macula densa is worth its salt. *J Clin Invest* 104: 1007–1009, 1999

26. Gadau J, Peters H, Kastner C, Kühn H, Nieminen-Kelhä M, Khadzhynov D, Krämer S, Castrop H, Bachmann S, Theilig F: Mechanisms of tubular volume retention in immune-mediated glomerulonephritis. *Kidney Int* 75: 699–710, 2009

27. Fernández-Llama P, Andrews P, Ecelbarger CA, Nielsen S, Knepper M: Concentrating defect in experimental nephrotic syndrone: Altered expression of aquaporins and thick ascending limb Na+ transporters. *Kidney Int* 54: 170–179, 1998

28. Marinelli RA, Tietz PS, Pham LD, Rueckert L, Agre P, LaRusso NF: Secretin induces the apical insertion of aquaporin-1 water channels in rat cholangiocytes. *Am J Physiol* 276: G280–G286, 1999

29. Leheste JR, Melsen F, Wellner M, Jansen P, Schlichting U, Renner-Müller I, Andreassen TT, Wolf E, Bachmann S, Nykjaer A, Willnow TE: Hypocalcemia and osteopathy in mice with kidney-specific megalin gene defect. *FASEB J* 17: 247–249, 2003

30. Christensen EI, Verroust PJ, Nielsen R: Receptor-mediated endocytosis in renal proximal tubule. *Pflugers Arch* 458: 1039–1048, 2009

31. Tietz PS, McNiven MA, Splinter PL, Huang BQ, Larusso NF: Cytoskeletal and motor proteins facilitate trafficking of AQP1-containing vesicles in cholangiocytes. *Biol Cell* 98: 43–52, 2006

32. Moeller HB, Olesen ET, Fenton RA: Regulation of the water channel aquaporin-2 by posttranslational modification. *Am J Physiol Renal Physiol* 300: F1062–F1073, 2011

33. Gunnarson E, Zelenina M, Aperia A: Regulation of brain aquaporins. *Neuroscience* 129: 947–955, 2004

34. Conner MT, Conner AC, Bland CE, Taylor LH, Brown JE, Parri HR, Bill RM: Rapid aquaporin translocation regulates cellular water flow: Mechanism of hypotonicity-induced subcellular localization of aquaporin 1 water channel. *J Biol Chem* 287: 11516–11525, 2012

35. Zhang W, Zitron E, Hömme M, Kihm L, Morath C, Scherer D, Hegge S, Thomas D, Schmitt CP, Zeier M, Katus H, Karle C, Schwenger V: Aquaporin-1 channel function is positively regulated by protein kinase C. *J Biol Chem* 282: 20933–20940, 2007

36. Han Z, Patil RV: Protein kinase A-dependent phosphorylation of aquaporin-1. *Biochem Biophys Res Commun* 273: 328–332, 2000

37. Baetz NW, Stamer WD, Yool AJ: Stimulation of aquaporin-mediated fluid transport by cyclic GMP in human retinal pigment epithelium in vitro. *Invest Ophthalmol Vis Sci* 53: 2127–2132, 2012

38. Kocinsky HS, Dynia DW, Wang T, Aronson PS: NHE3 phosphorylation at serines 552 and 605 does not directly affect NHE3 activity. *Am J Physiol Renal Physiol* 293: F212–F218, 2007

39. Duan Y, Gotoh N, Yan Q, Du Z, Weinstein AM, Wang T, Weinbaum S: Shear-induced reorganization of renal proximal tubule cell actin cytoskeleton and apical junctional complexes. *Proc Natl Acad Sci U S A* 105: 11418–11423, 2008

40. Acconcia F, Sigismund S, Polo S: Ubiquitin in trafficking: The network at work. *Exp Cell Res* 315: 1610–1618, 2009

41. Leitch V, Agre P, King LS: Altered ubiquitination and stability of aquaporin-1 in hypertonic stress. *Proc Natl Acad Sci U S A* 98: 2894–2898, 2001

42. Nedvetsky PI, Tabor V, Tamma G, Beulshausen S, Skroblin P, Kirschner A, Mutig K, Boltzen M, Petrucci O, Vossenkämper A, Wiesner B, Bachmann S, Rosenthal W, Klussmann E: Reciprocal regulation of aquaporin-2 abundance and degradation by protein kinase A and p38-MAP kinase. *J Am Soc Nephrol* 21: 1645–1656, 2010

43. Greger R, Hampel W: A modified system for in vitro perfusion of isolated renal tubules. *Pflugers Arch* 389: 175–176, 1981

44. Rickheit G, Wartosch L, Schaffer S, Stobrawa SM, Novarino G, Weinert S, Jentsch TJ: Role of ClC-5 in renal endocytosis is unique among ClC exchangers and does not require PY-motif-dependent ubiquitylation. *J Biol Chem* 285: 17595–17603, 2010

45. Kastner C, Pohl M, Sendeski M, Stange G, Wagner CA, Jensen B, Patzak A, Bachmann S, Theilig F: Effects of receptor-mediated endocytosis and tubular protein composition on volume retention in experimental glomerulonephritis. *Am J Physiol Renal Physiol* 296: F902–F911, 2009

46. Dardik A, Chen L, Frattini J, Asada H, Aziz F, Kudo FA, Sumpio BE: Differential effects of orbital and laminar shear stress on endothelial cells. *J Vasc Surg* 41: 869–880, 2005

47. Theilig F, Bostanjoglo M, Pavenstädt H, Grupp C, Holland G, Slosarek I, Gressner AM, Russwurm M, Koesling D, Bachmann S: Cellular distribution and function of soluble guanylyl cyclase in rat kidney and liver. *J Am Soc Nephrol* 12: 2209–2220, 2001

48. Theilig F, Kriz W, Jerichow T, Schrade P, Hähnel B, Willnow T, Le Hir M, Bachmann S: Abrogation of protein uptake through megalin-deficient proximal tubules does not safeguard against tubulointerstitial injury. *J Am Soc Nephrol* 18: 1824–1834, 2007